

2018

Heat Transfer and Pressure Drop of R1123/R32 Flow in Horizontal Microfin Tubes During Condensation and Evaporation

Chieko Kondou

Nagasaki Univ., Japan, ckondou@nagasaki-u.ac.jp

Shigeru Koyama

Kyushu University, Japan, koyama@cm.kyushu-u.ac.jp

Follow this and additional works at: <https://docs.lib.purdue.edu/iracc>

Kondou, Chieko and Koyama, Shigeru, "Heat Transfer and Pressure Drop of R1123/R32 Flow in Horizontal Microfin Tubes During Condensation and Evaporation" (2018). *International Refrigeration and Air Conditioning Conference*. Paper 1867.
<https://docs.lib.purdue.edu/iracc/1867>

This document has been made available through Purdue e-Pubs, a service of the Purdue University Libraries. Please contact epubs@purdue.edu for additional information.

Complete proceedings may be acquired in print and on CD-ROM directly from the Ray W. Herrick Laboratories at <https://engineering.purdue.edu/Herrick/Events/orderlit.html>

Heat Transfer and Pressure Drop of R1123/R32 Flow in Horizontal Microfin Tubes during Condensation and Evaporation

Chieko KONDOU ^{1*}, Shigeru KOYAMA ²

¹ Nagasaki University, Graduate School of Engineering,
Nagasaki, Japan
E-mail: ckondou@nagasaki-u.ac.jp

² Kyushu University, NEXT-RP in Int. Inst. for Carbon Neutral Energy Research,
Fukuoka, Japan
E-mail: koyama@cm.kyushu-u.ac.jp

* Corresponding Author

ABSTRACT

In this study, the heat transfer coefficient (HTC) and pressure drop of the new low global warming potential refrigerant mixture R1123/R32 (40/60 mass%) in a 6.0 mm OD horizontal microfin tube during condensation at 40 °C and evaporation at 10 °C are experimentally quantified. The data are then compared to the component R32. Both the condensation HTC and pressure drop of R1123/R32 (40/60 mass%) are somewhat lower than those of R32. Similarly, the pressure drop of R1123/R32 during the evaporation process at 10 °C is somewhat lower than that of R32. However, the evaporation HTC is comparable to that of R32. The lower surface tension of R1123/R32 can enhance the nucleate boiling and compensate the heat transfer degradation based on the difference in volatility

1. INTRODUCTION

For mitigation of global warming, a phase-down schedule of the production and the consumption amount of HFCs (Hydro Fluoro Carbons) and Hydro Chloro Fluoro Carbons (HCFCs) were specifically declared in the Kigali amendment (Heath, 2017) of the Montreal protocol. According to this schedule, by 2036, developed countries should reduce their equivalent amount of CO₂ by 85% from the baseline period of 2011 to 2013. Under these circumstances, low global warming potential (GWP) refrigerants have been attracting the attention of air conditioner and refrigerator manufacturers worldwide. The current commercial focus is mostly on Hydro Fluoro Olefins (HFOs) exhibiting a GWP of less than 1, with the acceptance of mild flammability. HFO-1123 (hereafter designated as R1123) is the one example. Although the use of R1123 alone causes the risk of a disproportionate reaction under very high pressure and temperature conditions, this substance has potentially beneficial thermophysical properties as a mixture component coupled with R32. A binary mixture, R1123/R32, is anticipated to be a new candidate R410A alternative used in stationary air conditioning systems. Nevertheless, the characteristics of the heat transfer and pressure drop of these refrigerants have not yet been clarified. As described in many previous studies (Thome, 1983; Jung and Radermacher, 1993; Niederküger and Steiner, 1994), volatility differences result in a severe degradation of the heat transfer coefficient (HTC). Therefore, to understand the transport phenomenon of these ternary mixtures, the HTC and pressure gradient during the evaporation process in a horizontal microfin tube are experimentally investigated in this study. Experimental data on R1123/R32 at a composition of 40/60 mass% are compared to R32 alone and to the predicted results based on the correlations proposed for other binary mixtures.

2. EXPERIMENTAL METHOD

2.1 Test loop

Fig. 1 (a) shows a vapor compression cycle facilitating the measurement of the HTC and pressure drop. The HTC and pressure drop are measured in the test section. To determine the bulk enthalpies of superheated vapor, the bulk

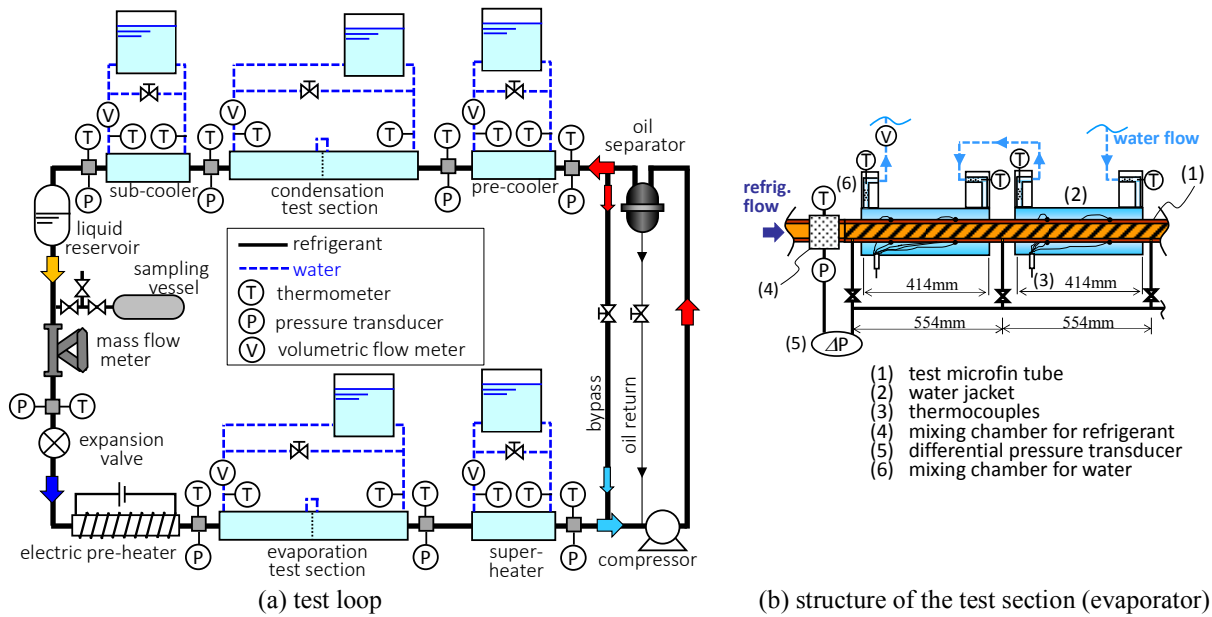


Figure 1: Experimental apparatus

mean temperature and pressure are measured in mixing chambers placed at the inlet of the pre-cooler and at the outlet of the super-heater. Additionally, the circulation composition is measured by sampling approximately 1 cc of subcooled liquid at the outlet of the liquid reservoir just after the data are recorded. The sampled liquid is completely vaporized in a sampling vessel, and then assayed using a thermal conductivity detector gas chromatograph. The refrigerant state is consistently evaluated under the circulation composition. Based on the bulk enthalpies of the superheated vapor, the enthalpies in the test sections are calculated by considering the enthalpy changes in the pre-cooler, super-heater, and the test section obtained from the water side heat balance.

Fig. 1 (b) illustrates the structure of the test section. A horizontally placed test microfin tube is surrounded by two water jackets and connected to the pressure ports for measuring the heat transfer rates over the 414-mm length and pressure drops at 554-mm intervals. At each subsection (i.e., the water jacket), eight thermocouples were embedded outside of the tube wall. The internal tube surface temperature, T_{wi} , was obtained from the measured outer tube temperature considering the one-dimensional heat conduction of the tube wall.

$$T_{wi} = (T_{wo,top} + T_{wo,bottom} + T_{wo,right} + T_{wo,left}) / 4 - [Q_{H2O\ TS} / (2\pi\Delta Z\lambda_{tube})] \ln(d_o / d_{eq}) \quad (1)$$

The representative refrigerant temperature of each subsection, $T_{r\ TS}$, is defined as the arithmetic mean of the inlet and outlet calculated from the enthalpies and pressures by assuming thermodynamic equilibrium.

$$T_{r\ TS} = (T_{r\ TS,i} + T_{r\ TS,o}) / 2 \quad (2)$$

$$T_{r\ TS,i} = f_{EOS}(h_{r\ TS,i}, P_{r\ TS,i}, X_{R1123}), \quad T_{r\ TS,o} = f_{EOS}(h_{r\ TS,o}, P_{r\ TS,o}, X_{R1123}) \quad (3)$$

Similarly, the representative vapor quality of each subsection, x , is calculated as follows:

$$x_{TS} = (x_{TS,i} + x_{TS,o}) / 2 \quad (4)$$

$$x_{TS,i} = f_{EOS}(h_{r\ TS,i}, P_{r\ TS,i}, X_{R1123}), \quad x_{TS,o} = f_{EOS}(h_{r\ TS,o}, P_{r\ TS,o}, X_{R1123}) \quad (5)$$

Based on the actual heat transfer area, the heat flux, q , and the HTC, α , are defined as follows:

$$\alpha_{TS1} = q_{TS1} / (T_{r\ TS1} - T_{wi}) \quad (6)$$

$$q_{TS1} = Q_{H2O\ TS1} / (\pi d_{eq} \eta_A \Delta Z) \quad (7)$$

A deviation of within 1 kW m⁻² of the targeted average heat flux was allowed to adjust for the test conditions, except for the dryout condition. An experiment is carried out at a pressure corresponding to the average of the bubble and dew temperatures equal to 40 °C for the condensation tests and 10 °C for evaporation tests.

2.2 Test Microfin Tube

Fig. 2 shows microscopic images of the cross-sectional area of the test microfin tube. The dimensions are specified in Table 1. The equivalent inner diameter, d_{eq} , is the diameter of a smooth tube that envelops an equally free flow volume. The surface enlargement, η_A , is the ratio of the actual heat transfer area to that of the equivalent smooth tube. In this study, the mass velocity is defined with a cross-sectional free flow area considering the helix angle. The HTC and heat flux also are defined using the actual heat transfer area.

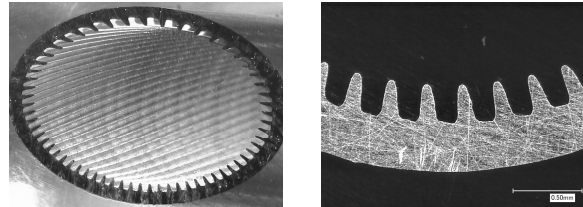


Figure 2: Sectional view of the tested microfin tube

Table 1: Dimensions of the test microfin tube

	Outer diameter	Equivalent inner diameter*	Wall thickness	Helix angle	Apex angle	Number of fins	Fin height	Area enlargement
	[mm]	[mm]	[mm]	[deg]	[deg]	[-]	[mm]	[-]
	6.03	5.21	0.324	18	15	30	0.269	2.62

* The diameter of an equivalent smooth tube envelops the same internal-free-flow-volume. That was obtained from the actual cross-sectional area A_{cross} and the helix angle β .
$$d_{eq} = \sqrt{(4A_{cross})/(\pi \cos \beta)}$$

2.3 Test Refrigerants

The test refrigerant mixture, R1123/R32 (40/60 mass%), was supplied by Asahi Glass Co., Ltd. The purity and nominal composition was more than 99.998 mol% and 39.3/60.7 mass%, respectively, according to the material sheet. Table 2 lists the thermophysical properties of R1123/R32 (40/60 mass%) evaluated at average saturation temperatures of 40 °C and 10 °C. By fitting the measured data, the equation of state was proposed for R1123 by Akasaka and Higashi (2016). Using this equation of state, the thermodynamic properties of the R1123/R32 (40/60 mass%) mixture are calculated using a mixture model (Kunz and Wagner, 2012) without excess energy through the mutual interaction designated as the KW0 model in REFPROP91 (Lemmon et al., 2013). The temperature glide of R1123/R32 (40/60 mass%) is 0.64 K at 40 °C and 1.1 K at 10 °C, which is significantly smaller than that of R32/R1234ze (E) (60/40 mass%). Thus, the heat transfer degradation by the mass transfer resistance owing to the difference in volatility is expected to be small. The surface tension is calculated as 8.27 mNm⁻¹ at 10 °C using an empirical correlation proposed based on the measured data by Kondou et al. (2018). The transport properties, namely, the liquid thermal conductivity and viscosity, are estimated using the extended corresponding state model (Klein et al., 1997; Huber et al., 1992). Because the mixing model and transport property correlations have yet to be established for the tested refrigerant mixture, it should be noted that the error in the measured and predicted results might be unexpectedly large.

Table 2: Thermophysical properties of the tested refrigerants

Average saturation temperature		at 40 °C		at 10 °C	
		R32	R1123/R32 (40/60 mass%)	R32	R1123/R32 (40/60 mass%)
Saturation pressure ^{*1}	MPa	2.48	2.84	1.11	1.31
Temperature glide ^{*1}	K	-	0.64	-	1.10
Density (vapor) ^{*1}	kg m ⁻³	73.3	105.8	30.2	43.1
Density (liquid) ^{*1}		893	891	1020	1036
Latent heat ^{*1}	kJ kg ⁻¹	237	175	299	236
Surface tension ^{*2}	mN m ⁻¹	4.489	3.60	9.26	8.27
Viscosity (liquid) ^{*3}	μPa s	95.0	88.2	134.6	126.3
Thermal conductivity (liquid) ^{*3}	mW m ⁻¹ K ⁻¹	115	92.7	137	113

*1 - calculated using REFPROP9.1 KW0 default model with R1123 EOS of Akasaka and Higashi (2016)

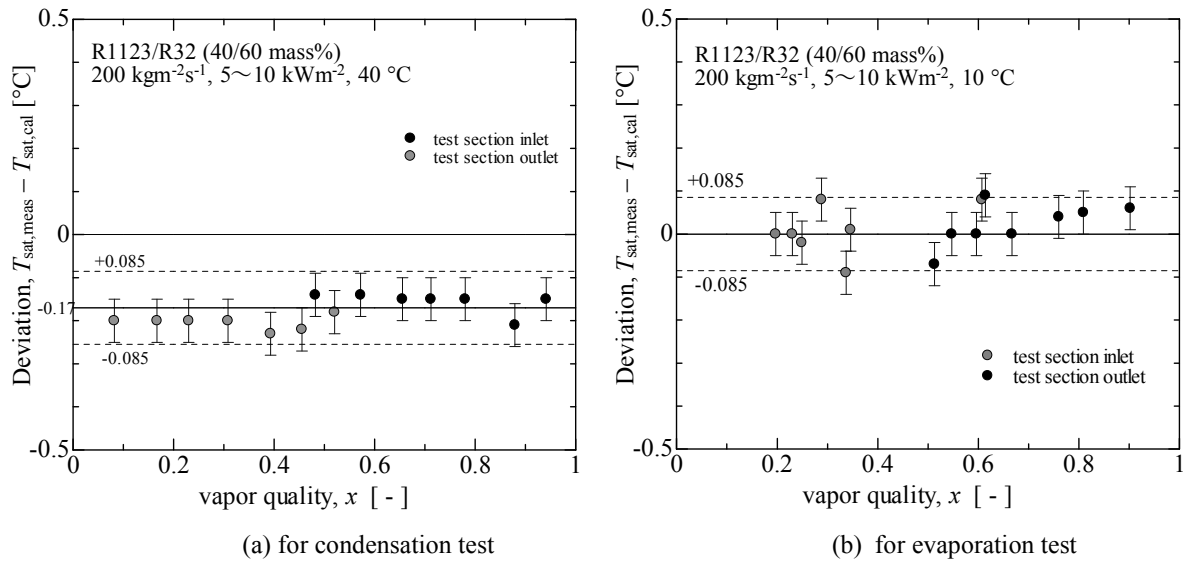


Figure 3: Refrigerant saturation temperature check

*2 - calculated using the empirical correlation of Kondou et al. (2018)
 *3 - estimated using the ECS model provided by REFPROP9.1 (Klein et al., 1997; Huber et al., 1992)

2.4 Refrigerant Saturation Temperature

The saturation temperature of the mixtures depends on the composition, pressure, and vapor quality. This means the temperature can include a larger uncertainty. Thus, the saturation temperature should be carefully obtained for the new mixture, the property data of which have not been adequately reported.

For a validation of the method determining the saturation temperature, Fig. 3 plots the deviation in the measured bulk mean refrigerant temperature calculated using the KW0 model provided by REFPROP9.1. The bulk mean refrigerant temperatures are measured in mixing chambers placed at the test section inlet and outlet with an uncertainty of approximately ± 0.05 K. The calculated refrigerant temperature corresponds to the saturation temperature at the measured local pressure and the obtained enthalpy. The uncertainty in the calculated temperature is typically ± 0.085 K. As shown in Fig. 3 (a), the measured temperature negatively deviates from the calculation at a saturation temperature of 40 °C. The same tendency is shown for both the test section inlet and outlet. The average deviation is consistently -0.17 K. It appears to be that the mixing model, which has not yet been optimized for R1123/R32, results in a slightly higher saturation temperature than the true value. Based on this, an offset of -0.17 K in the saturation temperature was chosen for the condensation test. Fig. 3 (b) shows the results at an average saturation temperature of 10 °C. The measured refrigerant temperature randomly deviates because of the larger fluctuation in the measured pressure during the evaporation test. Nevertheless, no obvious or systematic deviation, or bias, was shown, and most of the data agree with the calculated temperature within the uncertainty. Fortunately, the default KW0 model gives almost the exact temperature at 10 °C. Therefore, in this study, for the evaporation test, the saturation temperature is simply calculated using the KW0 model without an offset.

3. RESULTS AND DISCUSSION

3.2 HTC and Pressure Drop of R1123/R32 (40/60 mass%)

Figs. 5(a) and 5(b) show the condensation HTC and pressure drop, respectively, as a function of the liquid quality, which were experimentally quantified for R1123/R32 (40/60 mass%) at a heat flux of 10 kWm⁻² and pressure of 2.84 MPa corresponding to an average saturation temperature of 40 °C, and a mass velocity of 200 to 400 kg m⁻²s⁻¹. The bars appended to the symbols show the propagated measurement uncertainty (Taylor, 1997) in the HTC or the pressure drop in the vertical direction, and the vapor quality over a subsection in the horizontal direction. The lines indicate the predicted HTC and pressured drop based on the correlations of Yonemoto-Koyama (2007) and Silver-Bell-Ghaly (1988) when considering the heat transfer degradation owing to the volatility difference, and based on Baba (2013) for the pressure drop, DP/DZ . The variation in measured HTC agrees well with the predicted value

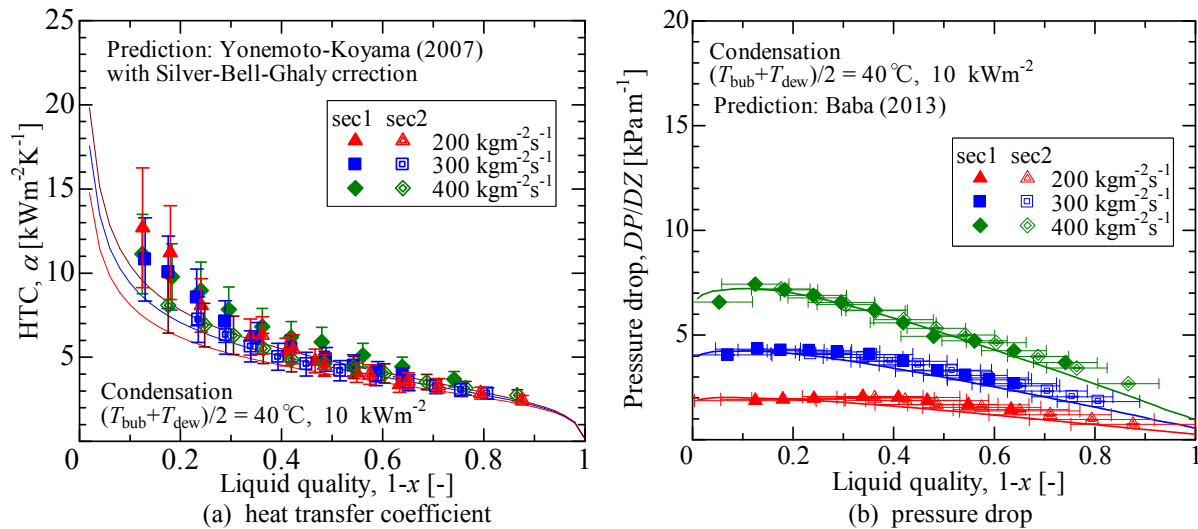


Figure 5: R1123/R32 (40/60 mass%) condensation test results at various mass velocities

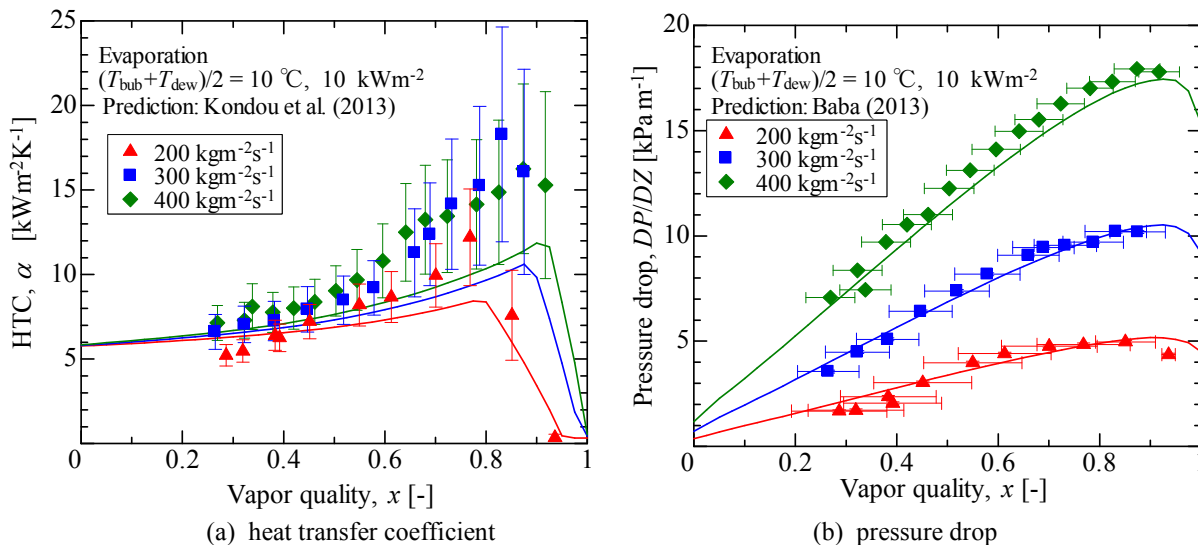


Figure 6: R1123/R32 (40/60 mass%) evaporation test results at various mass velocities

except at liquid qualities of less than 0.2, where the uncertainty becomes notably large. In addition, the measured pressure drop agrees with the prediction within the measurement uncertainty.

Figs. 6(a) and 6(b) show the evaporation HTC and the pressure drop, respectively, as a function of vapor quality at a pressure of 1.31 MPa corresponding to an average saturation temperature of $10\text{ }^{\circ}\text{C}$, and a mass velocity of 200 to $400\text{ kg m}^{-2}\text{s}^{-1}$. The HTC increases with an increase in vapor quality, and then sharply decreases under a vapor quality of approximately 0.8, which indicates a typical dryout occurrence in a horizontal tube. Similarly, the pressure drop increases with the increase in vapor quality of up to 0.9 and then gradually decreases or plateaus. The measured data are compared to the existing predictions, which are shown with the solid lines in Figs. 6(a) and 6(b). For HTC in a dryout region of other single components is selected. For the pressure drop, the correlation of Baba (2013) proposed for R32/R1234ze(E) is selected. Although the selected correlation underestimates the HTC at vapor qualities of 0.6 to 0.9, a reasonable prediction is given at lower vapor qualities and in the dryout region at a mass velocity of 200, 300, and $400\text{ kg m}^{-2}\text{s}^{-1}$. On the other hand, the correlation of Baba provides a precise prediction in the entire measured region.

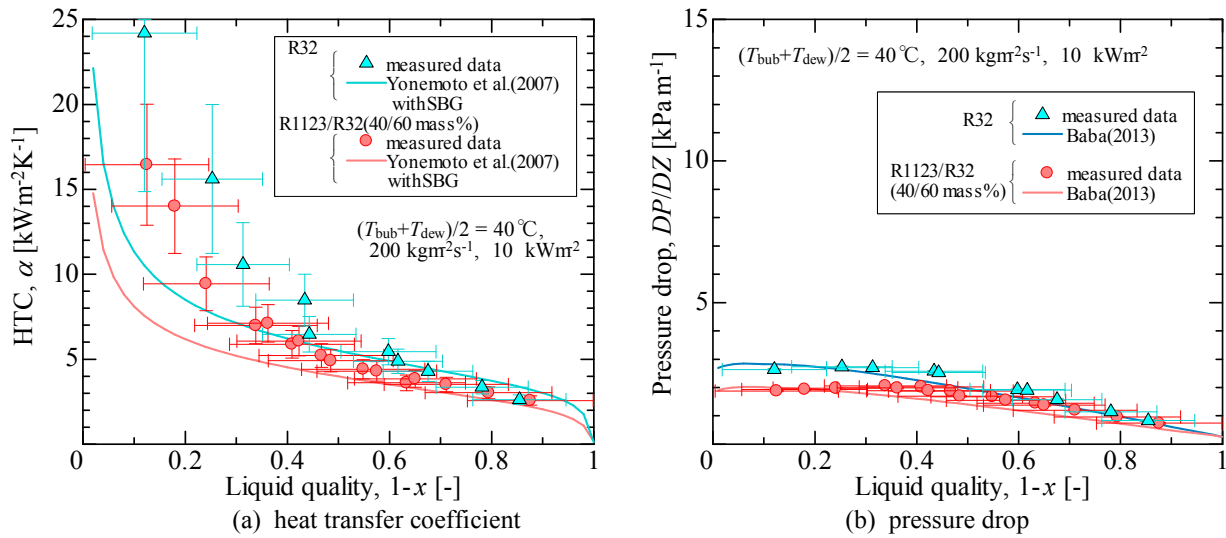


Figure 7: Comparison between R1123/R32(40/60 mass%) and R32 at 40 °C

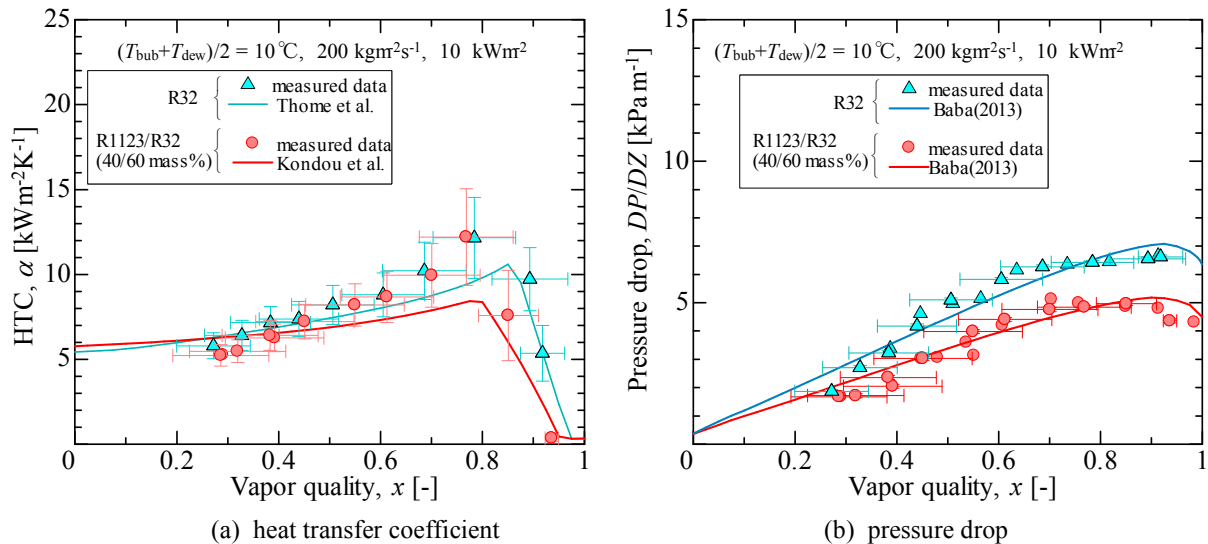


Figure 8: Comparison between R1123/R32(40/60 mass%) and R32 at 10 °C

3.3 Comparison between R1123/R32 (40/60 mass%) and R32 alone

Figs. 7 and 8 compare the condensation and evaporation HTC and the pressure drop between R1123/R32 (40/60 mass%) and the component R32 at average temperatures of 40 °C and 10 °C, a mass velocity of 200 kg m⁻² s⁻¹, and a heat flux of 10 kW m⁻².

The condensation HTC of R1123/R32 (40/60 mass%) is somewhat lower than that of the component R32 alone. This can be explained through the higher liquid thermal conductivity and lower vapor density of R32, as specified in Table 2. At a given mass velocity, the lower vapor density indicates a higher vapor velocity, and a greater convective contribution can be expected in the condensation heat transfer, which is also helped by the higher thermal conductivity. Instead, the pressure drop of R32 becomes somewhat higher than that of R1123/R32 (40/60 mass%). The heat transfer degradation caused by the mass transfer resistance is not severe for R1123/R32 (40/60 mass%). These characteristics seem to be well explained based on the predictions plotted by the solid lines.

The evaporation HTC of R1123/R32 (40/60 mass%) is almost comparable to that of R32 alone. One reason for this is the much lower surface tension of R1123/R32 (40/60 mass%) than that of R32, as shown in Table 2. This can enhance the nucleate boiling contribution in the evaporation HTC. The HTC is predicted using the thermodynamic

properties, and the estimated transport properties still agree satisfactorily with the measured data for both refrigerants. At present, the effects of the transport properties, e.g., the thermal conductivity, are unclear because of a lack in precise measurement data. The pressure drop of R1123/R32 (40/60 mass%) is clearly lower than that of R32 alone owing to the slower vapor velocity from the higher vapor density. The correlation of Baba shows a high degree of overlap with the measured pressure drop data and reasonably reflects the effects of the vapor velocity. Further discussions, such as the viscosity effect of the pressure drop, will be available when the transport property measurement data are reported for this mixture.

4. CONCLUSIONS

The HTC and pressure drop in a horizontal microfin tube with an outer diameter of 6.0 mm are experimentally qualified for a newly nominated low GWP refrigerant mixture, R1123/R32, at a nominal composition of 40/60 mass%, and an average saturation temperature of 40 °C in the condensation test and 10 °C in the evaporation test. The condensation HTC at 40 °C was somewhat lower than that of R32. The evaporation HTC of R1123/R32 (40/60 mass%) was almost comparable to that of R32 alone, which suggests that the heat transfer degradation by the mass transfer resistance is notably small compared to other recently proposed mixtures. In the evaporation heat transfer, the smaller surface tension of R1123/R32 enhances the nucleate boiling and compensates the mass transfer resistance. On the other hand, the pressure drop of R1123/R32 (40/60 mass%) during both condensation and evaporation is obviously lower than that of R32 because of the higher vapor density. At the present stage, the mixing model is still being developed, and transport property measurements are ongoing for R1123/R32. The more specific contribution of the model will be revealed when it becomes better established.

REFERENCES

- Heath, E., 2017. Amendment to the Montreal Protocol on Substances that Deplete the Ozone Layer (Kigali Amendment). *International Legal Materials*, 56(1), 193-205.
- Jung, D., Radermacher, R., 1993, Prediction of evaporation heat transfer coefficient and pressure drop of refrigerant mixtures in horizontal tubes, *Int. J. Refrig.*, vol. 16: p. 201-209.
- Niederhäuser, M., Steiner, D., 1994, Flow boiling heat transfer to saturated pure components and non-azeotropic mixtures in a horizontal tube, *Chem. Eng. Prog.*, vol. 33: p. 261-275.
- Thome, J.R. 1983. Prediction of binary mixture boiling heat transfer coefficients using only phase equilibrium data. *International Journal of Heat and Mass Transfer* 26(7):965–74.
- Kunz, O. and Wagner, W. The GERG-2008 Wide-Range Equation of State for Natural Gases and Other Mixtures: An Expansion of GERG-2004. *J. Chem. Eng. Data*, 57(11):3032-3091, 2012.
- Klein, S.A., McLinden, M.O., Laesecke, A. (1997). An improved extended corresponding states method for estimation of viscosity of pure refrigerants and mixtures. *Int. J. Refrigeration*, 20: 208-217.
- Huber, M.L., Friend, D.G., Ely, J.F., 1992. Prediction of the thermal conductivity of refrigerants and refrigerant mixtures. *Fluid Phase Equilibria*, 80: 249-261.
- Higashi, Y., Akasaka, R., 2016. Measurements of Thermodynamic Properties for HFO-1123 and HFO-1123 + R32 Mixture. 15th International Refrigeration and Air Conditioning Conference at Purdue, West Lafayette, IN, July 11-14, Paper 1688.
- Lemmon, E.W., Huber, M.L., McLinden, M.O., 2013, Reference Fluid Thermodynamic and Transport Properties - REFPROP Ver. 9.1, National Institute of Standards and Technology, Boulder, CO, USA.
- Taylor, J.T. 1997. *An Introduction to Error Analysis*, 2nd ed, pp. 73–75. University Science Book.
- Kondou, C., Matsuzono, T., Tsuyashima, T., Higashi, Y., 2018. Surface tension measurement of low GWP refrigerant mixture HFO-1123/HFC-32, The 9th Asian Conference on Refrigeration and Air Conditioning ACRA2018 June 11-13, 2018, Sapporo, JAPAN.
- Kondou, C., BaBa, D., Mishima, F., Koyama, S., 2013. Flow boiling of non-azeotropic mixture R32/R1234ze (E) in horizontal microfin tubes. *Int. J. Refrig.* 36, 2366–2378.
- Yoshida, S., Mori, H, Kakimoto, Y., Ohishi, K., 2000. Dryout quality for refrigerants flowing in horizontal evaporator tubes. *Trans. JSRAE*, 4:511–20 (in Japanese)
- Baba, D., 2013. An experimental study on condensation and evaporation of low GWP refrigerants in microfin tubes. Doctor thesis, Kyushu University, Inter disciplinary Graduate School of Engineering Sciences, (in Japanese)

- Thome, J.R., Kattan, N., Favrat, D., 1997, Evaporation in microfin tubes: a generalized prediction model, Proc. Convective Flow and Pool Boiling Conf., Kloster Irsee, Germany, Paper VII-4.
- Klein, S.A., McLinden, M.O. and Laesecke, A. (1997). An improved extended corresponding states method for estimation of viscosity of pure refrigerants and mixtures. Int. J. Refrigeration 20: 208-217.
- Huber, M.L., Friend, D.G. and Ely, J.F. Prediction of the thermal conductivity of refrigerants and refrigerant mixtures. Fluid Phase Equilibria 80: 249-261 (1992).
- Kunz, O. and Wagner, W. The GERG-2008 Wide-Range Equation of State for Natural Gases and Other Mixtures: An Expansion of GERG-2004. J. Chem. Eng. Data, 57(11):3032-3091, 2012.
- Silver, L. (1947). Gas cooling with aqueous condensation. Trans. Inst. Chem. Engrs., 25, 30-42.
- Bell, K. J., & Ghaly, M. A. An approximate generalized design method for multicomponent/partial condenser, AIChE Symp. Ser. 69(1973) 72-79.

NOMENCLATURE

P	pressure	(kPa)
Q	heat transfer rate	(W)
T	temperature	($^{\circ}$ C)
X	circulation mass fraction	(-)
ΔZ	effective heating length	(m)
d_o	outer diameter	(m)
d_{eq}	equivalent inner diameter	(m)
h	enthalpy	(Jkg ⁻¹)
h_{fin}	fin height	(m)
q	heat flux	(Wm ⁻²)
x	vapor quality	(-)
α	heat transfer coefficient	(Wm ⁻² K ⁻¹)
λ	thermal conductivity	(Wm ⁻¹ K ⁻¹)
η_A	enlargement ratio of heat transfer surface	(-)

Subscript

top	top
bottom	bottom
left	left
right	right
H ₂ O	water
r	refrigerant
i	inlet
o	outlet
R1123	R1123
tube	tube
TS	test section
wi	inner tube wall
wo	outer tube wall
EOS	equation of state

ACKNOWLEDGEMENTS

The sample refrigerants were kindly donated by Asahi Glass Co., Ltd., Japan. The test microfin tube was kindly provided by Kobelco and Materials Copper Tube, Ltd. This study was financially supported by the New Energy and Industrial Technology Development Organization (NEDO). The authors thankfully acknowledge their support. The authors also thank Mr. Okada Takahiro for his valuable effort regarding the experiment.